ACS APPLIED MATERIALS & INTERFACES

RESEARCH ARTICLE

www.acsami.org

Eruption Combustion Synthesis of NiO/Ni Nanocomposites with Enhanced Properties for Dye-Absorption and Lithium Storage

Wei Wen and Jin-Ming Wu*

State Key Laboratory of Silicon Materials, Zhejiang University, Hangzhou, 310027, P. R. China

Supporting Information

ABSTRACT: Large-scale energy-efficient productions of oxide nanoparticles are of great importance in energy and environmental applications. In nature, volcano eruptions create large amounts of volcano ashes within a short duration. Inspired by such phenomena, we report herein our first attempt to achieve an artificial volcano for mass productions of various oxide nanoparticles with enhanced properties for energy and environmental applications. The introduction of NaF into the solution combustion synthesis (SCS), which is a generally adopted synthetic route for mass productions of various oxide nanoparticles, results in better particle dispersity and a drastic increase in specific surface area compared to the conventional SCS. In a fixed dosage of NaF, a new eruption combustion pattern emerges, which may be contributed to the more gas evolution, lower apparent density, and weaker interparticle force. The novel eruption combustion pattern observed in SCS provides a versatile alternative for SCS to control combustion behavior, microstructure, and property of the products. NiO/Ni nanocomposite yielded by the new approach shows an ideal dye-absorption ability as well as lithium storage capacity. The new SCS pattern reported in this paper is versatile, emerging in various systems of Ni−Co−O, Co−O, La−O, Ni−Co−O, Zn−Co−O, and La−Ni−O.

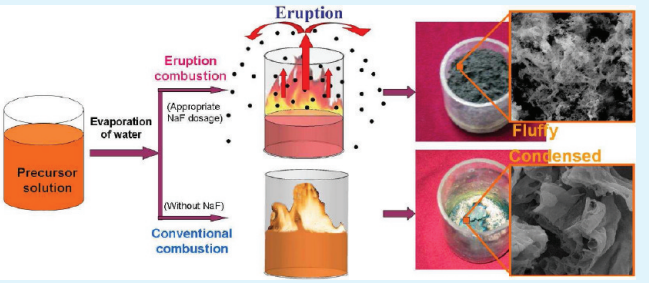

KEYWORDS: nanoparticles, combustion synthesis, lithium ion battery, adsorption, eruption

1. INTRODUCTION

In the past decade, nanomaterials have sparked worldwide interest due to their unique physical and chemical properties in comparison with those of their bulk counterparts. Nowadays, many techniques, such as coprecipitation, electrodeposition, sol-gel chemistry, and solvothermal route, have been developed to synthesize materials in nanoscale, but these strategies are always high-energy consuming and require rather long reaction times. Solution combustion synthesis (SCS), which is self-sustained by its own exothermic reaction, is an effective, rapid, and energy-efficient method for mass productions of various nanocrystalline oxides.[1−4] Nowadays, SCS becomes more and more popular, finding practical applications in more than 65 countries.[5] In SCS, the precursors are often environmentally benign and can be mixed on the molecular level compared to conventional self-propagating high-temperature synthesis.[6] The composition of products can be tailored simply by varying the precursor.[7] Substantive gas evolution during the combustion reaction leads to porous morphology and high specific area in products. Because of these advantages, materials by SCS have received outstanding properties for applications in catalysis,[8,9] photoluminescence,[10,11] and Li-ion battery.[12,13] Nanoparticles of pure metals and alloys were also achieved successfully by SCS,[14−16] further displaying the superiority of this synthesis strategy. More recently, combustion synthesis was further developed to serve as a general route to achieve diverse electronic metal oxide films at temperatures as low as 200 °C, which allows one to fabricate transistors with high-performance on flexible plastic substrates.[17]

In SCS, the phase and morphology of products can be controlled by fuel selection and fuel-to-oxidant ratio. The fuel-to-oxidant ratio also affects the combustion mode, that is, volume combustion synthesis or self-propagating high-temperature synthesis, which is categorized by the rate of temperature increase (dT/dt), the maximum temperature (T_{max}), and the duration of combustion (t).[18−20] In the volume combustion synthesis (VCS), the reaction occurs simultaneously in the solution volume with high dT/dt, high T_{max}, and short t. For the self-propagating high-temperature synthesis (SHS), the combustion occurs locally and then propagates through the reaction volume. The later achieves generally powders with higher surface area.[18−20] However, controlling the combustion pattern[21] remains one of the most challenging tasks for SCS. There remains very little room for the conventional SCS to promote the surface area of the products. In this paper, we describe a new type of combustion pattern in SCS, the so-called eruption combustion, which provides an alternative for SCS to tune the combustion behavior, microstructure, and property of the products.

Received: July 30, 2011
Accepted: September 15, 2011
Published: September 15, 2011

dx.doi.org/10.1021/am2010064 | ACS Appl. Mater. Interfaces 2011, 3, 4112–4119

NiO/Ni nanocomposites are important materials for various applications in bioseparations[22] and Li-ion batteries.[23,24] Their magnetic properties have also been studied extensively.[25,26] In this report, we take the synthesis of NiO/Ni as an example to demonstrate the novel eruption combustion pattern in SCS for mass productions of nanoparticulate oxides with enhanced properties. Compared with conventional SCS, the introduction of NaF into the solution combustion synthesis resulted in smaller particles, improved dispersity, and remarkably increased specific surface area. By adjusting the NaF dosage, a new eruption combustion pattern was observed. NiO/Ni nanocomposite yielded by the new approach shows an ideal dye-absorption ability as well as lithium storage capacity. In addition, we have shown that this new combustion pattern can be applied to systems other than Ni−O, such as Ni−Co−O, Co−O, Zn−Co−O, La−O, and La−Ni−O systems, which is therefore of general interest to researchers exploring nanoparticles for various applications in energy storage and environmental remediation.

2. EXPERIMENTAL SECTION

2.1. Synthesis. All reagents were of analytical grade and used as received without further purifications. In a typical synthesis, $Ni(NO_3)_2 \cdot 6H_2O$ (20 mmol), citric acid ($C_6H_8O_7 \cdot H_2O$, 11 mmol), and a certain amount of NaF (0, 10, 15, 20, 22, 25, 30 mmol) were dissolved in deionized water (20 mL) in a quartz container (50 mm in out diameter), which was then transferred to a preheated furnace maintained at 400 °C with the oven port opened. Within a few minutes, the solution boiled and was ignited to produce a self-propagating combustion. The powders were then washed with deionized water and absolute ethanol three times, respectively, and dried at 80 °C in air overnight. The temperature rise in the combustion process was measured using a type K thermocouple. To exclude the impact of heating effects from the oven, once the reaction was triggered, the crucible was taken out from the oven, leaving the reaction self-sustained.

2.2. Characterization. X-ray diffraction (XRD) measurements were conducted on a Rigaku D/max-3B diffractometer with Cu Kα radiation, operated at 40 kV, 100 mA (λ = 0.15406 nm). Quantitative analysis of the relative content of Ni and NiO phases was made by means of a reference intensity ratio (RIR) method using the XRD patterns. The powder morphology was observed using a field emission scanning electron microscopy (FE-SEM, Hitachi S-4800, Tokyo, Japan), equipped with an energy dispersive X-ray analysis (EDS) system. Transmission electron microscopy (TEM) observation was conducted employing a JEM-2010 microscope (JEOL, Japan) working at 200 kV. The Brunauer-Emmett-Teller (BET) approach using adsorption data was utilized to determine the specific surface area. The sample was degassed at 150 °C for 14 h to remove physisorbed gases prior to the measurement. An STA-449F3 (NETZSCH-Gerätebau GmbH, Germany) was used to conduct differential scanning calorimetry (DSC) and thermogravimetric analysis (TGA) of gels obtained by quenching before being ignited at a heating rate of 4 K/min from 300 to 873 K in argon atmosphere.

2.3. Adsorption Experiment. The adsorbent sample (0.2 g) was added to methylene blue solution (100 mL) with an initial concentration of 30 μM under mechanical stirring. After 30 minutes, the solid and liquid were separated centrifugally, and the residual methylene blue concentration was determined by UV-visible spectrophotometry at 663 nm.

2.4. Lithium Storage Test. The working electrodes were prepared by a slurry coating procedure. The slurry consisted of 80 wt % active materials, 15 wt % acetylene black, and 5 wt % polyvinylidene fluoride (PVDF) dissolved in *N*-methyl pyrrolidinone (NMP, and was coated on a nickel foam of 1.5 cm in diameter, which acted as a current collector.

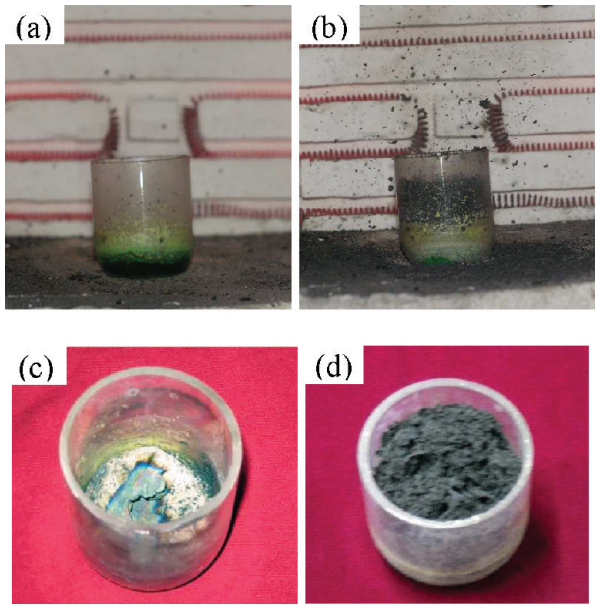

Figure 1. (a, b) Eruption combustion process (φ = 1.00) and photographs of the products for φ = 0 (c) and φ = 1.00 (d), respectively.

The foam was pressed under a pressure of 20 MPa after drying at 90 °C for 12 h in vacuum. The cells were assembled in an argon-filled glove box using Li foil as a counter electrode and polypropylene (PP) film (Celgard 2300) as a separator. The electrolyte was 1M $LiPF_6$ in a 50:50 (w/w) mixture of ethylene carbonate (EC) and diethyl carbonate (DEC). The charge−discharge tests were conducted on a BS-9390 battery program-control test system at a constant current of 0.2 C (71.8 mA/g) between 3.0 V and 0.02 V.

3. RESULTS AND DISCUSSION

3.1. Eruption Combustion. In a typical procedure, we use citric acid as a fuel and a complexing agent and nickel nitrate hexahydrate as an oxidant. Differently from conventional SCS, we additionally employ NaF to serve as a control agent for the combustion behavior. Here, the fuel to oxidant ratio remains stoichiometric of 5/9, which means that all oxygen required for fuel combustion derives from the oxidant. The molar ratio of NaF to metal ions, denoted as φ, is the only variant, where φ = 0 implies a conventional SCS. Varying the value of φ from 0 to 1.50, it is observed that combustion occurs locally and further propagates through the reaction volume, which is characteristic of the SHS mode (see movies in Supporting Information). By adding appropriate amounts of NaF (φ = 0.75−1.10), it can be seen that lots of powders were lifted off and naturally fall down around the container, leaving highly fluffy products with a quite big volume (see Figure 1b,d and a movie in Supporting Information). On the contrary, the common SCS procedure resulted in compact products with remarkably smaller volume (Figure 1c, and a movie in Supporting Information). The phenomenon observed in the current investigation is very similar to a volcano eruption in nature, in which volcano ash is ejected to an altitude of several kilometers. The emergence of such an eruption behavior may be attributed to the following key points arising from the NaF additives: large flow rate of gas evolution, relatively low apparent density, and weak interparticle forces. On the basis of the above features, materials produced by this

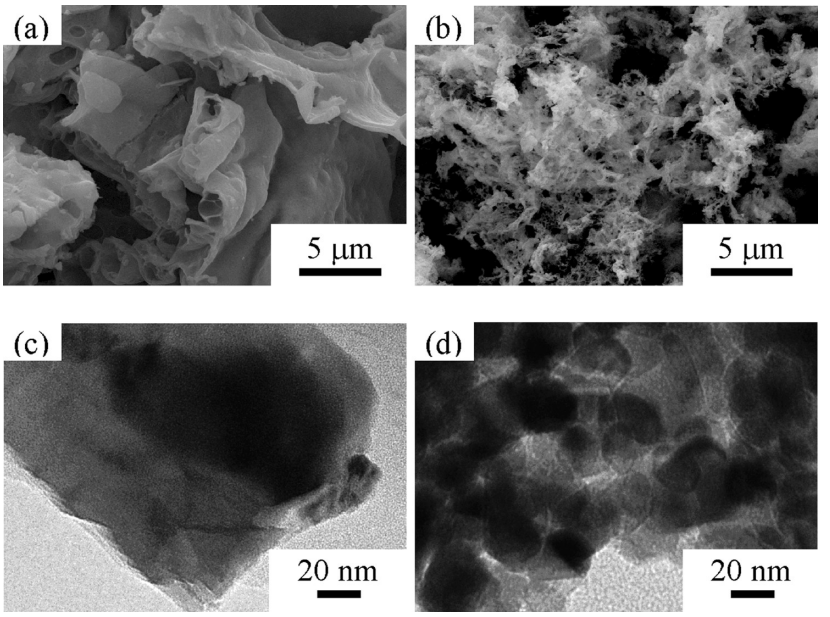

Figure 2. SEM and TEM images of the washed products derived with φ = 0 (a, c) and φ = 1.00 (b, d), respectively.

strategy must have small particle size, good dispersity, and high specific surface area. The whole synthesis process was completed just within a few minutes, and the only external thermal energy input needed is for dehydration of the precursor solution and for igniting the combustion reaction. It is also worth mentioning that the yield in the current eruption solution combustion is relatively high compared to the conventional SCS, in which precursors around the vessel wall always combust incompletely. Besides, the products obtained by the eruption combustion are so "lithe" that no grinding is demanded before all the characterizations performed in the current investigation. When compared with the conventional SCS, which usually emerges explosive behaviors, the eruption combustion synthesis reported in our work is relatively slower and more moderate in a self-propagating mode. In industrial, the spill of nanoparticles can be restricted by simply covering a dense metal grid over the container.

Figure 2a depicts typical aggregates derived by the conventional SCS (φ = 0), which illustrates tight three-dimensional flakes with dozens of micrometers in size. The flakes possessed a smooth surface. With the additive of certain NaF into the precursor solution (φ = 1.00), the three-dimensional flake structure was broken up and switched to highly fluffy and porous networks consisting of fine nanoparticles (Figure 2b). Figure 2c, d shows typical TEM images of the above two samples. The particle size of the former is several hundred nanometers; while the latter is only 20−30 nm.

Combining the highly fluffy and porous structure with the dramatically reduced particle size, the product (NiO/Ni nanocomposite, as will be demonstrated in Figure 4a later) derived from the eruption combustion procedure possessed a high specific surface area of 20.6 m^2/g, which is nearly 8 times that of the one obtained by conventional SCS (2.6 m^2/g), as demonstrated in Figure 3. More interestingly, only the nanoparticles derived by the present eruption combustion exhibited a type IV nitrogen isotherm with a type H3 desorption hysteresis loop, indicating the existence of mesopores,[27] which is in good accordance with the SEM observation (Figure 2b). Previous literature indicated that it is extremely difficult to obtain Ni or

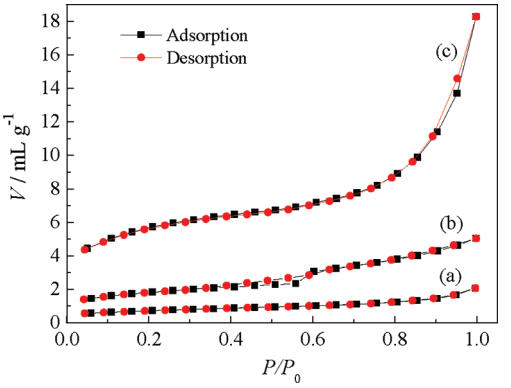

Figure 3. Nitrogen adsorption−desorption isotherm of NiO/Ni nanoparticles yielded by (a) conventional SCS (φ = 0), (b) salt-assisted SCS (NaCl, φ = 1.00), and (c) eruption combustion synthesis (NaF, φ = 1.00).

NiO particles with high surface area via SCS.[15,28] For example, the specific surface area of Ni and Ni-based alloys obtained by Erri et al. using SCS were in the range of 0.8−3.5 m^2/g.[15] Prasad et al. reported that the surface area of $Ce_{0.75}Zr_{0.25}O_2$ powders obtained by SCS decreased from 29.2 to 5.5 m^2/g after introducing NiO.[28] Recently, salt-assisted solution combustion synthesis (SSCS) has been developed to achieve enhanced dispersity and surface area of products compared with conventional SCS.[29] We also used NaCl, a typical salt used in SSCS, to assist the synthesis of NiO/Ni particles (the photograph, SEM, and XRD for the products are shown in Figure S1 in Supporting Information). The surface area is promoted to a value of 6.5 m^2/g, which is still much smaller than that achieved by the present eruption combustion. The density of NiO and Ni are 6.7 and 8.9 g/cm^3, respectively. It can thus be anticipated that the specific surface area of the nanocomposites increases slightly with increasing NiO content. The NiO contents of the powders derived by conventional SCS, salt-assisted SCS, and the present eruption combustion synthesis are 32%, 60%, and 79% (see Figure 4b and

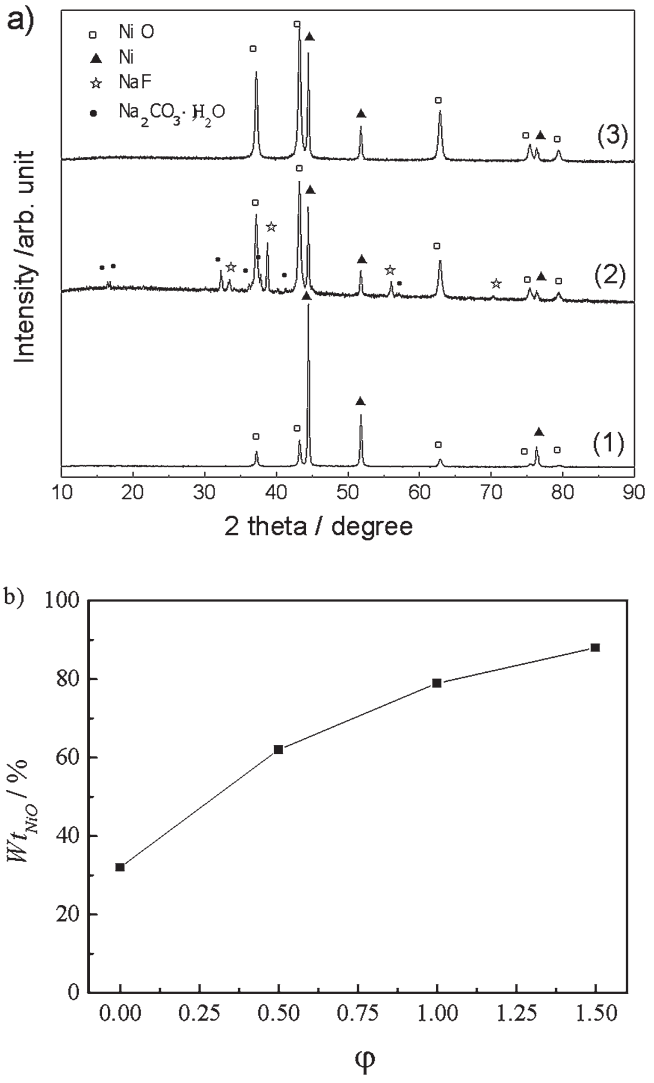

Figure 4. (a) XRD patterns of the products: (1) φ = 0 and washed, (2) φ = 1.00 and unwashed, and (3) φ = 1.00 and washed. (b) The dependence of mass percent of NiO in the products on φ, the ratio of NaF to nickel ions.

Figure S1 in Supporting Information); however, such a difference in NiO content cannot explain solely the distinct specific surface area as illustrated in Figure 3. The dramatic increase in the specific surface area should be contributed to the additive of NaF and its resultant eruption combustion.

The phase composition of the products derived using φ = 0 and 1.00 is determined by XRD measurements. After washing, both patterns show Bragg reflection of NiO and Ni phases (patterns 1 and 3 in Figures 4a); however, the relative amount of NiO is significantly different. Figure 4b indicates the mass percentage of NiO in the NiO/Ni composite powders as a function of φ. It is clear that the relative amount of NiO increased with increasing amounts of the NaF additives. The mass percent of NiO increased from 32% to 88% by varying φ from 0 to 1.50. For the unwashed products from the eruption combustion, there are byproducts indexed to NaF and $Na_2CO_3 \cdot H_2O$ (pattern 2 in Figure 4a). The mappings of five elements of Ni, O, Na, F, and C, as illustrated in Figure 5, demonstrate homogeneous distributions of them all around the sample, indicating that both NaF and $Na_2CO_3 \cdot H_2O$ uniformly distributed around the NiO/Ni particles and formed a continuous salt matrix. This inhibited efficiently the agglomeration of the newly formed products, resulting in well-dispersed nanoparticles.[27] Thus, the introduction of NaF is in favor of improving the surface area of the products. As illustrated in Figure S2 in Supporting Information, it can be seen that the surface area of products increases with increasing NaF dosage. With the increasing NaF dosage, the NiO content increases (Figure 4b), which may slightly contribute to the increasing surface area.

In the self-propagating high-temperature synthesis, the additive of alkali-metal salts has been found to reduce effectively the particle size, because the melt of the inert salt additive serves to lower the overall temperature and to promote the diffusion of the reactants,[30,31] but no smooth continuous surfaces expected for alkali-metal salt melt can be observed for the unwashed product (see the SEM image in Figure 5). Actually, the maximum temperature encountered in the present eruption was far below the melting point of both NaF (1266 K) and Na_2CO_3 (1124 K) (see Figure 6). Hence, melting of the alkali-metal salts does not happen in this eruption combustion process. Different from the alkali-metal salts in previous reports,[30] the NaF additive is not really "inert" because of its partial conversions to $Na_2CO_3 \cdot H_2O$ as indicated by the XRD pattern (pattern 2 in Figure 4a and also Figure S3 in Supporting Information). The deep involvement of NaF in the combustion procedure may favor a more oxidative atmosphere, which resulted in the increasing NiO content with increasing amounts of the NaF additive (Figure 4b). Interestingly, Lesnikovich et al. also observed the presence of heat-resistant sodium carbonate in a new type of self-organization in combustion, that is, the incandescent liquid spheroidal formation.[21]

The exact route from NaF to Na_2CO_3 is not clear at the present time; however, such a reaction involving NaF may absorb some heat, which results in a lower overall temperature (Figure 6), favoring the prevention of products from sintering and agglomerating. Moreover, such highly soluble alkali-metal salts are cheap and easily removable from the as-combusted products simply by washing (patterns 2 and 3 in Figure 4a and Figure S4 in Supporting Information), which therefore does not deteriorate the purity of products. As mentioned above, the eruption combustion may be attributed to the large flow rate of gas evolution and the low procedure temperature, as well as the homogeneously distributed salts. Therefore, this phenomenon can emerge only in fixed conditions (φ = 0.75-1.10, as indicated in Figure 6). The eruption disappeared in case that the amounts of NaF were either less or more. Figure S5 in the Supporting Information shows the products derived using φ = 0.50 and 1.50, in which the eruption combustion did not occur. However, when compared to the sample derived without the NaF additive (Figure 2a), the broken of the three-dimensional flake structure to dispersed particles is also obvious because of the NaF additive, which explains the improvement in the specific surface area (Figure S2 in Supporting Information).

To well understand the combustion process, we carried out thermogravimetry (TG) and differential scanning calorimetry (DSC) investigations in argon atmosphere at a heating rate of 4 K/min to characterize the gels obtained by quenching before igniting in presence and absence of the NaF additive. As exhibited in Figure 7a,b, the two gels show similar TG-DSC curves. For both samples, unlike conventional solution synthesis routes such as sol-gel, which exhibit a broad endothermal peak contributing to the product formation and organic removal,[17]

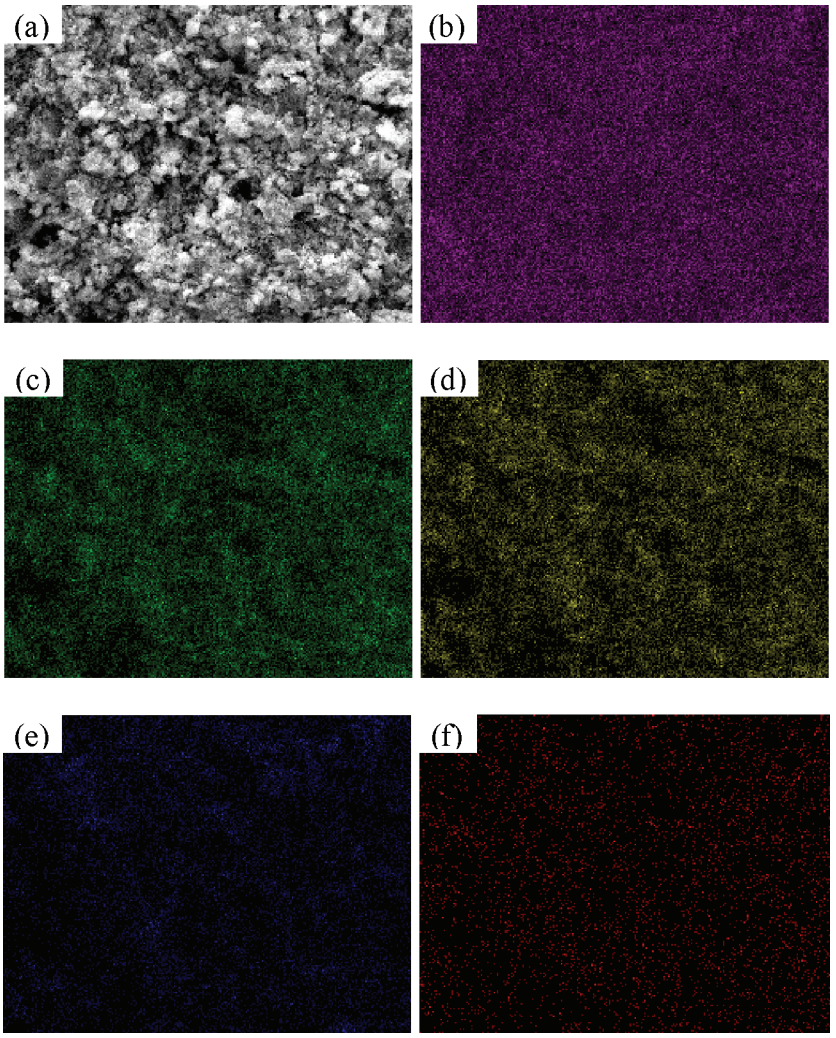

Figure 5. (a) The as-combusted product (φ = 1.00) and the corresponding mappings of (b) Ni, (c) O, (d) Na, (e) F, and (f) C.

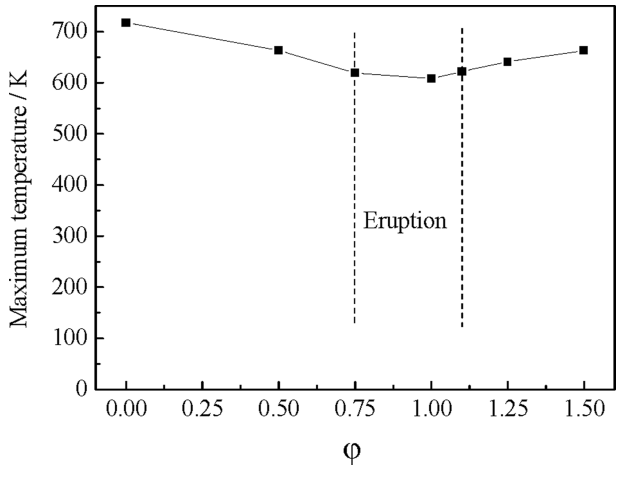

Figure 6. Dependence of maximum temperature on φ, the ratio of NaF to nickel ions.

a large exothermic peak was observed from 433 to 456 K accompanied by an abrupt loss in weight, which is attributed to the combustion reaction of the gel. These results reveal that the NaF additive has no obvious effects on both the ignition temperature and the driving force for the SCS. The ignition temperature is determined by the specific decomposition temperature of one of the reagents in the solution (oxidant or/and fuel).[1,16] In these systems, the exothermic peak is close to the decomposition temperature of nickel nitrate hexahydrate[16,32] and is slightly lower than the decomposition temperature of citric acid.[1] Hence, the combustion process may be ignited by the reaction of HNO_3 and NO_2 species resulting from the decomposition of nickel nitrate hexahydrate with citric acid. More details of the synthesis process are shown by the time-temperature profile of the combustion process (Figure 7c), which suggests that the synthesis process can be divided into five stages. Stage I: the solution was heated from room temperature to boiling; Stage II: the evaporation of water resulted in the temperature of the solution remaining at 100 °C unchanged; Stage III: after complete dehydration, the resulting xerogel continued to be heated; Stage IV: once the temperature reached the ignition temperature, the precursor was ignited and the combustion reaction occurred, resulting in the sudden rise of the temperature and lattice formation; Stage V: natural cooling. The difference in the ignition temperature observed in the TG-DSC curve and the time−temperature profile can be contributed to the difference in the response rate for the temperature

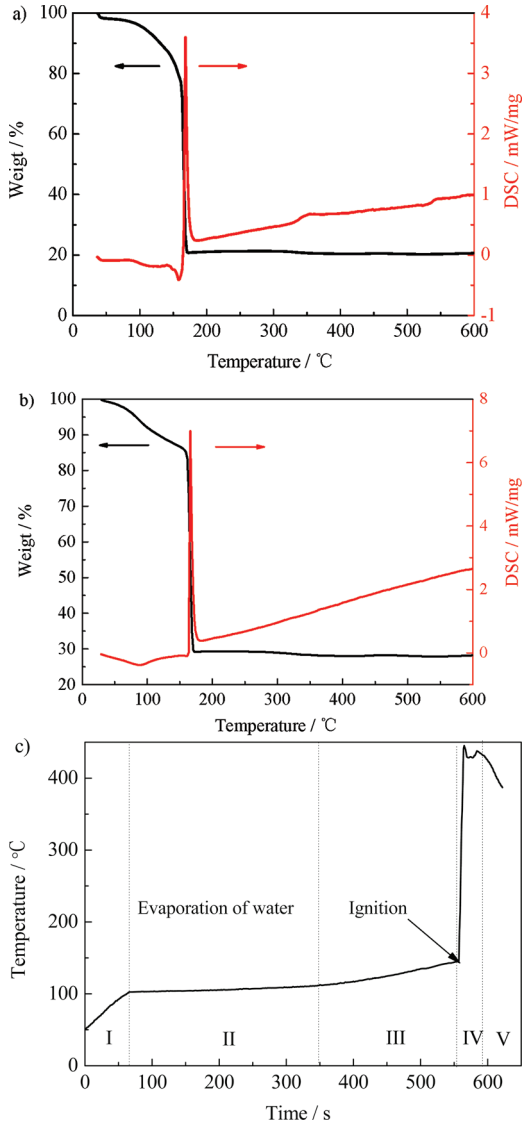

Figure 7. TG-DSC curves of the gels obtained by quenching before being ignited in argon atmosphere at a heating rate of 4 K/min: (a) $\varphi = 0$, (b) $\varphi = 1.00$. (c) Typical time−temperature profile of the combustion process for $\varphi = 0$.

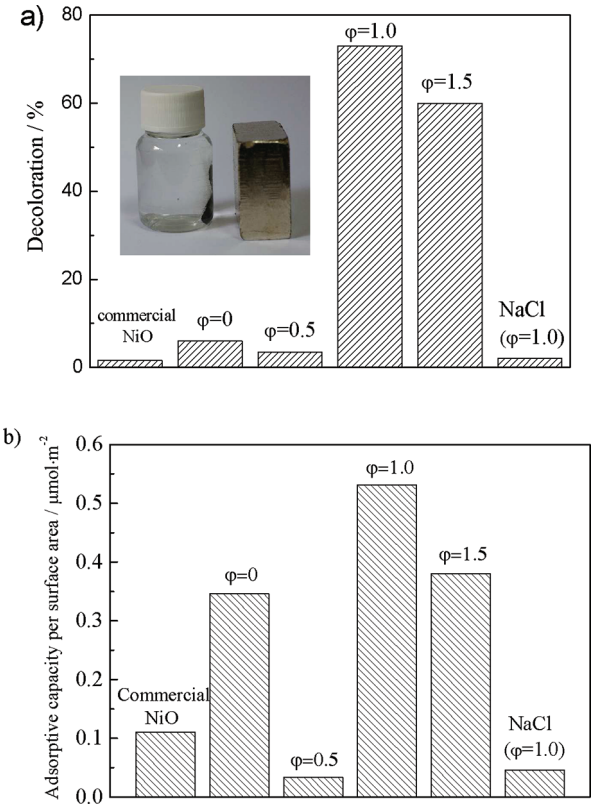

Figure 8. Bar plot showing the removal of methylene blue in dark for 30 min in solutions equilibrated with NiO/Ni derived using $\varphi = 0$, 0.50, 1.00, and 1.50, the commercial NiO, and NiO/Ni derived by NaCl-assisted solution combustion synthesis (the molar ratio of NaCl to nickel ions is 1.00): (a) decoloration and (b) adsorptive capacity per surface area. The inset in (a) is a photograph showing magnetic recycle of the NiO/Ni nanoparticles ($\varphi = 1.00$).

measurment. The driving force in SCS derives from internal chemical energy, which is from the highly exothermic redox reaction. The primary energy consumption is just used for dehydration of the precursor solution, and the required temperature can be depicted as that for the reaction initiation. Therefore, the temperature needed in SCS is just higher than the ignition temperature (160 °C in the present case), making the synthesis route energy-saving.

3.2. Dye Absorption. Motivated by its fluffy and porous structure, we expected that the NiO/Ni nanoparticles derived from the present eruption combustion process would be useful in wastewater treatment, which is an emerging yet challenging task at present time. NiO has been utilized as a photocatalyst or adsorbent for toxic chromium and dyes in wastewater.[33−35] Unlike activated carbon, the metal oxides adsorbent can be reused by being combusted at relatively low temperatures.[35,36] Methylene blue (MB), which is widely used in the paper, textile, leather, and printing industries and also a popular probe in photocatalysis, was used as a probe of the surface adsorption ability in the current investigation. After 30 min equilibration, ca. 73% and 60% of the initial MB molecules were removed by adsorption on the NiO/Ni nanoparticles for $\varphi = 1.00$ and $\varphi = 1.50$. All the other NiO/Ni nanoparticles derived by $\varphi = 0$, 0.50, NaCl-assisted solution combustion synthesis, and the commercial NiO nanoparticles (see Figure S6 (Supporting Information) for the morphology of the commercial NiO) showed negligible ability of the dye absorption (Figure 8a). For the five NiO/Ni nanoparticles achieved by SCS, the absorption ability of the two derived utilizing $\varphi = 1.00$ and $\varphi = 1.50$ was significantly higher than the others. This can be explained by their higher fractions of NiO (Figure 4b). Compared to $\varphi = 1.00$, the sample with $\varphi = 1.50$ possessed even higher NiO fraction and higher surface area but lower absorption ability; therefore, the fluffy and porous structure resulted from the eruption combustion benefited significantly from the dye-absorption ability. The amounts of absorbed MB molecules were normalized with surface area of the absorbents, which was illustrated in Figure 8b. The specific surface area of the commercial NiO nanopowders was measured to be 2.1 m^2/g, and the other values were derived from Figure 3 and Figure S2 in Supporting Information. It can be seen that the decoloration is not directly proportional to the surface area. This can be contributed to the fact that, other than surface area, many factors such as microstructure and surface chemistry are also

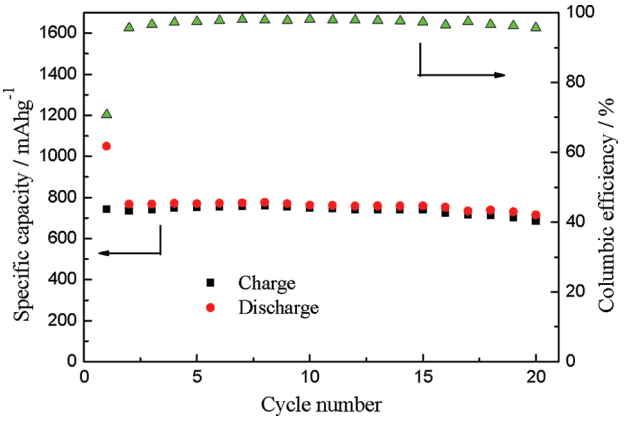

Figure 9. Cycle performance of NiO/Ni anode electrode (φ = 1.00) at a current density of 71.8 mA/g.

of significant importance for the dye-adsorption.[3] The NiO/Ni nanoparticles derived by the eruption combustion exhibited the most remarkable absorption ability even after normalizing with the surface area, which evidenced the advantages of the present novel combustion mode for dye-absorption applications. This may be partly contributed to the unique porous structure resulting from the eruption combustion. Furthermore, the solid/liquid separation is fairly easy, as the NiO/Ni nanoparticles dispersed in water (φ = 1.00) can be easily attracted using a magnet due to its paramagnetic behavior (see the inset in Figure 8a).

3.3. Lithium Storage. NiO has also been considered to be ideal materials to construct negative electrodes for rechargeable lithium-ion batteries (LIBs) because of its high theoretic specific capacity (718 mAh/g), environmental friendliness, low cost, and natural abundance.[37−40] As another example of potential applications, we performed lithium storage tests using the NiO/Ni nanoparticles derived by the present eruption combustion procedure as an anode material due to its simple, low cost, and large scale synthesis. The reaction mechanism of NiO with Li in lithium-ion batteries was proposed as follows[39]

$$NiO + 2Li \underset{\text{charge}}{\overset{\text{discharge}}{\rightleftharpoons}} Li_2O + Ni$$

Hence, the presence of Ni nanoparticles facilitates the more complete decomposition of the Li_2O and solid electrolyte interface (SEI) in the charge process, and the Ni phase also improves the electric conductivity.[23] The lithium storage tests were performed at a constant current of 0.2 C (1 C is defined as one lithium per formula in an hour, that is 359 mA/g for NiO) in a potential window of 0.02−3.0 V versus Li. Figure 9 shows that the second charge capacity is 743 (mA·h)/g and the charge capacity at the end of the 20th cycle is 702 (mA·h)/g that approaches the theoretical value of 718 (mA·h)/g with a retention of 94%. Moreover, the coulomb efficiency with a high initial value of 70.8% keeps a value over 96% during the cycle. It is noted that the capacity of nanosheet-based NiO microspheres decreased sharply to a neglectable level after 8 cycles at 50 mA/g in the potential range of 0.01−3.0 V.[41] The nanoparticles provide short diffusion lengths for lithium ions, and the Ni phase improves also the electric conductivity. The fluffy porous structure here not only buffers the volume change during cycling but also facilitates the efficient ingress and infiltration of the electrolyte into the electrode and diffusion of the ions, which in turn contributes to the excellent lithium storage performance.

By transplanting the above synthesis parameters (namely, φ = 1.00 and the ratio of the citric acid fuel to oxidant keeps stoichiometric) to the Ni−Co−O system (Ni/Co = 1/2), the eruption combustion pattern also emerges (see Figure S7 in Supporting Information) for the comparison in the appearance of products derived by φ = 0 and φ = 1.00). More generally, this new type of eruption combustion synthesis is also applicable to Co−O, La−O, Ni−Co−O, Zn−Co−O, and La−Ni−O systems. Further studies for exploring the applicability of the novel strategy to fabricate other materials associated with their corresponding applications, and those on the detailed mechanism of the eruption combustion procedure, are ongoing.

4. CONCLUSION

We developed a new type of eruption combustion in SCS by introduction of appropriate NaF dosages into the precursor. The additive of NaF led to NiO/Ni nanocomposite powders with porous networks and in turn improved specific surface area. The eruption combustion occurred when appropriate amounts of NaF were used. NiO/Ni nanocomposite yielded by this new strategy showed an ideal dye-absorption ability as well as lithium storage capacity. This new pattern also appears in Ni−Co−O, Co−O, La−O, Ni−Co−O, Zn−Co−O, and La−Ni−O systems. The new combustion pattern reported herein provides an alternative to control the composition, microstructure, and property of the products.

■ ASSOCIATED CONTENT

Supporting Information. Photographs, XRD, SEM, EDS, BET, and two multimedia movies showing the combustion synthesis. This material is available free of charge via the Internet at http://pubs.acs.org.

■ AUTHOR INFORMATION

Corresponding Author
*E-mail: msewjm@zju.edu.cn.

■ REFERENCES

(1) Deshpande, K.; Mukasyan, A.; Varma, A. *Chem. Mater.* **2004**, *16*, 4896.
(2) Tao, X. Y.; Wang, X. N.; Li, X. D. *Nano Lett.* **2007**, *7*, 3172.
(3) Morales, W.; Cason, M.; Aina, O.; Tacconi, N. R. D.; Rajeshwar, K. *J. Am. Chem. Soc.* **2008**, *130*, 6318.
(4) Wu, J. M.; Wen, W. *Environ. Sci. Technol.* **2010**, *44*, 9123.
(5) Aruna, S. T.; Mukasyan, A. S. *Curr. Opin. Solid State Mater. Sci.* **2008**, *12*, 44.
(6) Rajeshwar, K.; Tacconi, N. R. D. *Chem. Soc. Rev.* **2009**, *38*, 1984.
(7) Hegde, M. S.; Madras, G.; Patil, K. C. *Acc. Chem. Res.* **2009**, *42*, 704.
(8) Nagaveni, K.; Hegde, M. S.; Ravishankar, N.; Subbanna, G. N.; Madras, G. *Langmuir* **2004**, *20*, 2900.
(9) Guo, X. M.; Mao, D. S.; Lu, G. Z.; Wang, S.; Wu, G. S. *J. Catal.* **2010**, *271*, 178.
(10) Saradhi, M. P.; Varadaraju, U. V. *Chem. Mater.* **2006**, *18*, 5267.
(11) Qiu, Z.; Zhou, Y.; Lu, M.; Zhang, A.; Ma, Q. *Acta Mater.* **2007**, *55*, 2615.
(12) Prakash, A. S.; Manikandan, P.; Ramesha, K.; Sathiya, M.; Tarascon, J. M.; Shukla, A. K. *Chem. Mater.* **2010**, *22*, 2857.
(13) Kalaiselvi, N.; Manthiram, A. *J. Power Sources* **2010**, *195*, 2894.
(14) Jiang, Y. W.; Yang, S. G.; Hua, Z. H.; Huang, H. B. *Angew. Chem.* **2009**, *121*, 8681.

(15) Erri, P.; Nader, J.; Varma, A. *Adv. Mater.* **2008**, *20*, 1243.
(16) Kumar, A.; Wolf, E. E.; Mukasyan, A. S. *AIChE J.* **2010**, *57*, 2207.
(17) Kim, M. G.; Kanatzidis, M. G.; Facchetti, A.; Marks, T. J. *Nat. Mater.* **2011**, *10*, 382.
(18) Mukasyan, A. S.; Costello, C.; Sherlock, K. P.; Lafarga, D.; Varma, A. *Sep. Purif. Technol.* **2001**, *25*, 117.
(19) Mukasyan, A. S.; Epstein, P.; Dinka, P. *Proc. Combust. Inst.* **2007**, *31*, 1789.
(20) Striker, T.; Ruud, J. A. *J. Am. Ceram. Soc.* **2010**, *93*, 2622.
(21) Lesnikovich, A. I.; Sviridov, V. V.; Printsev, G. V.; Ivashkevich, O. A.; Gaponik, P. N. *Nature* **1986**, *323*, 706.
(22) Lee, I. S.; Lee, N.; Park, J.; Kim, B. H.; Yi, Y. W.; Kim, T.; Kim, T. K.; Lee, I. H.; Paik, S. R.; Hyeon, T. *J. Am. Chem. Soc.* **2006**, *128*, 10658.
(23) Huang, X. H.; Tu, J. P.; Zhang, B.; Zhang, C. Q.; Li, Y.; Yuan, Y. F.; Wu, H. M. *J. Power Sources* **2006**, *161*, 541.
(24) Li, X. F.; Dhanabalan, A.; Bechtold, K.; Wang, C. L. *Electrochem. Commun.* **2010**, *12*, 1222.
(25) Salgueiriño-Maceira, V.; Correa-Duarte, M. A.; Bañobre-LÓpez, M.; Grzelczak, M.; Farle, M.; Liz-Marzán, L. M.; Rivas, J. *Adv. Funct. Mater.* **2008**, *18*, 616.
(26) Johnston-Peck, A. C.; Wang, J.; Tracy, J. B. *ACS Nano* **2009**, *3*, 1077.
(27) Wu, J. M. *Environ. Sci. Technol.* **2007**, *41*, 1723.
(28) Prasad, D. H.; Jung, H. Y.; Jung, H. G.; Kim, B. K.; Lee, H. W.; Lee, J. H. *Mater. Lett.* **2008**, *62*, 587.
(29) Tong, Y. P.; Zhao, S. B.; Wang, X.; Lu, L. D. *J. Alloys Compd.* **2009**, *479*, 746.
(30) Wiley, J. B.; Kaner, R. B. *Science* **1992**, *255*, 1093.
(31) Xia, B.; Lenggoro, I. W.; Okuyama, K. *Chem. Mater.* **2002**, *14*, 2623.
(32) Brockner, W.; Ehrhardt, C.; Gjikaj, M. *Thermochim. Acta* **2007**, *456*, 64.
(33) Song, X. F.; Gao, L. *J. Am. Ceram. Soc.* **2008**, *91*, 4105.
(34) Song, X. F.; Gao, L. *J. Phys. Chem. C* **2008**, *112*, 15299.
(35) Song, Z.; Chen, L. F.; Hu, J. C.; Richards, R. *Nanotechnology* **2009**, *20*, 275707 (9 pp).
(36) Zhong, L. S.; Hu, J. S.; Liang, H. P.; Cao, A. M.; Song, W. G.; Wan, L. J. *Adv. Mater.* **2006**, *18*, 2426.
(37) Armand, M.; Tarascon, J. M. *Nature* **2008**, *451*, 652.
(38) Liu, C.; Li, F.; Ma, L. P.; Cheng, H. M. *Adv. Mater.* **2010**, *22*, 28.
(39) Poizot, P.; Laruelle, S.; Grugeon, S.; Dupont, L.; Tarascon, J. M. *Nature* **2000**, *407*, 496.
(40) Cabana, J.; Monconduit, L.; Larcher, D.; Palacín, M. R. *Adv. Mater.* **2010**, *22*, E170.
(41) Liu, L.; Li, Y.; Yuan, S. M.; Ge, M.; Ren, M. M.; Sun, C. S.; Zhou, Z. *J. Phys. Chem. C* **2010**, *114*, 251–255.